Steady-State and Multiple Cracking of Short Random Fiber Composites

By Victor C. Li,[1] Member, ASCE, and Christopher K. Y. Leung[2]

Abstract: This paper analyzes the pseudostrain-hardening phenomenon of brittle matrix composites reinforced with discontinuous flexible and randomly distributed fibers, based on a cohesive crack-mechanics approach. The first crack strength and strain are derived in terms of fiber, matrix, and interface micromechanical properties. Conditions for steady-state cracking and multiple cracking are found to depend on two nondimensionalized parameters that embody all relevant material micromechanical parameters. The results are therefore quite general and applicable to a variety of composite-material systems. Phrased in terms of a failure-mechanism map, various uniaxial load-deformation behaviors for discontinuous fiber composites can be predicted. The influence of a snubbing effect due to local fiber/matrix interaction for randomly oriented crack-bridging fibers on the composite properties is also studied.

Introduction

In brittle-matrix composites reinforced with continuous fibers, a tensile failure strain higher than that of the matrix material has been observed at first crack. In addition, subsequent multiple cracking further extends the pseudostrain-hardening behavior in the intrinsically brittle matrix. In contrast, randomly oriented short-fiber–reinforced composites generally fail in a tension-softening mode at the initiation of a first crack. The processing ease, relatively low processing cost, and the isotropic mechanical properties of short-fiber composites, however, is a significant advantage over continuous reinforcements. A composite employing discontinuous fibers with the attendant processing advantage of discontinuous-fiber composites, together with the ductility performance of continuous reinforcements, would be extremely desirable. It has been pointed out (Aveston and Kelly 1973; Morton and Grove 1976; Brandt 1985; Li et al. 1990) that fiber/matrix local interactions due to inclined fiber pullout in randomly distributed fiber composites can produce crack-bridging forces that may partially compensate the well-known reduction in reinforcement efficiency due to bridging fiber number and discontinuity loss.

In this paper, we examine the conditions under which such a discontinuous random-fiber composite may exhibit some of the desirable features of continuously reinforced composites. These conditions are cast in terms of nondimensionalized microstructural parameters. The analysis shows that a single parameter $\bar{K}$, identified as a ratio between crack-tip and fiber-bridging toughness, determines the transition from a catastrophic failure mode to a stable failure mode. The presence or absence of multiple cracking is shown to depend on a combination of $\bar{K}$ and a nondimensionalized flaw size $\bar{c}$. A

[1]Assoc. Prof., Advanced Civ. Engrg. Materials Res. Lab., Dept. of Civ. and Envir. Engrg., Univ. of Michigan, Ann Arbor, MI 48109-2125

[2]Asst. Prof., Dept. of Civ. Engrg., Massachusetts Inst. of Tech., Cambridge, MA 02912.

Note. Discussion open until April 1, 1993. To extend the closing date one month, a written request must be filed with the ASCE Manager of Journals. The manuscript for this paper was submitted for review and possible publication on August 21, 1991. This paper is part of the ***Journal of Engineering Mechanics***, Vol. 118, No. 11, November, 1992. ©ASCE, ISSN 0733-9399/92/0011-2246/$1.00 + $.15 per page. Paper No. 2500.

mechanism map is devised showing a variety of possible failure modes in uniaxial tension.

Our approach would be to utilize the influence of fiber reinforcement, represented as a cohesive traction acting across the crack flanks, as a growing fracture resistance with crack extension. This toughening effect due to fiber bridging not only increases the composite first-crack strength, but also leads to a phenomenon known as steady-state cracking. Steady-state cracking occurs as a result of the balance between the composite toughness increase and the stress-intensity-factor increase due to applied load during crack extension, and is a prerequisite of multiple cracking or pseudostrain hardening. It occurs only if the stress-transfer capability of the reinforcing fibers is adequate. The analytic development of the theory of steady-state and multiple cracking in the present work draws heavily on elementary results from fracture mechanics. Broek (1986), for example, provides a nice treatment on the subject.

Bridging Stress-Crack–Opening Relationship

The bridging stress-crack–opening relationship (hereafter abbreviated as the σ_B-δ curve) results from fibers bridging across a matrix crack. In this paper, without loss of generality, we adopt a simple model of fiber pullout with only frictional constraint. That is, fibers are held in the matrix by friction with little or no elastic interfacial bond. Furthermore, we assume that the fibers are short enough (or with low enough interfacial friction) that all fibers will be pulled out without rupture. Consider a single fiber with an embedded length of l. During frictional debonding, the fiber bridging load P versus crack opening δ may be obtained from a shear-lag analysis:

$$P(\delta) = \frac{\pi}{2}\sqrt{(1+\eta)E_f d_f^3 \tau \delta}\, e^{f\phi} \qquad (\text{for } \delta \le \delta_0) \quad \ldots\ldots\ldots\ldots\ldots\ldots (1)$$

where $\delta_0 \equiv (4l^2\tau)/[(1+\eta)E_f d_f]$ corresponds to the crack opening at which frictional debonding is completed for a fiber with embedment length of l, diameter d_f, elastic modulus E_f, and with an interfacial frictional bond strength τ. In addition $\eta \equiv (V_f E_f)/(V_m E_m)$, where V_f, V_m = the fiber and matrix volume fractions, and E_f, E_m = the fiber- and matrix-elastic moduli, respectively.

When the fiber is fully debonded, the load-point displacement is mainly due to that of the fiber end slippage, and (for simplicity) we assume that the elastic stretching of the fiber can be neglected. This results in a fiber pullout load versus displacement relation given by

$$P(\delta) = \pi\tau l d_f \left(1 - \frac{\delta}{l}\right) e^{f\phi} \qquad \left(\text{for } \frac{l}{2} \ge \delta > \delta_0\right) \quad \ldots\ldots\ldots\ldots\ldots\ldots (2)$$

The exponential function in (1) and (2) is introduced to account for the snubbing effect (Li et al. 1990) that amplifies the bridging force due to fiber/matrix snubbing for a fiber originally inclined at an angle ϕ to the loading axis. The snubbing coefficient f is specific to a particular pairing of fiber and matrix. f has been experimentally measured to have a value between 0.5 and 1 for three fiber types in a cement matrix (Li et al. 1990; Li 1992). The snubbing mechanism is probably a good representation of the actual behavior for flexible (low modulus and/or small diameter for low bending stiffness, and high rupture strain) fibers. For brittle fibers with high stiffness,

a separate analysis performed by Leung and Li (1992) reveals potential fiber rupture or matrix spalling, rendering the snubbing mechanism unusable. The effect of fiber inclination on bridging force of fibers affect the resulting σ_B-δ curve only [(4) next]. The fundamental aspects of the analysis of first-crack strength and multiple cracking in the subsequent sections of this paper remains valid even for fiber/matrix systems that do not conform to the description in (1) and (2).

Li et al. (1991) show that the composite σ_B-δ curve can be predicted by integrating over the contributions of individual fibers crossing a matrix-crack plane:

$$\sigma_B(\delta) = \frac{4V_f}{\pi d_f^2}\int_{\phi=0}^{\pi/2}\int_{z=0}^{Lf/2\cos\phi} P(\delta)p(\phi)p(z)\, dz\, d\phi \quad \ldots\ldots\ldots\ldots\ldots\ldots (3)$$

where $p(\phi)$ and $p(z)$ = probability-density functions of the orientation angle and centroidal distance of fibers from the crack plane. For uniform three-dimensional (3-D) random distributions, $p(\phi) = \sin\phi$, and $p(z) = 2/L_f$, where L_f = the fiber length. Deviations from distribution randomness such as those due to processing/fabrication or deliberate bias introduction in fiber orientation requires modification of the expressions for $p(\phi)$ from the sine function and could easily be incorporated into (3).

At small crack opening, some fibers will undergo debonding [governed by (1)], while other fibers with short embedment length will undergo slippage [governed by (2)]. The composite bridging stress may be derived from (3), and together with (1) and (2), can be expressed in normalized form:

$$\tilde{\sigma}_B(\tilde{\delta}) = g\left[2\left(\frac{\tilde{\delta}}{\tilde{\delta}^*}\right)^{1/2} - \frac{\tilde{\delta}}{\tilde{\delta}^*}\right] \qquad (\text{for } \tilde{\delta} \le \tilde{\delta}^*) \quad \ldots\ldots\ldots\ldots\ldots\ldots (4)$$

where $\tilde{\sigma}_B \equiv \sigma_B/\sigma_0$ and $\sigma_0 \equiv V_f\tau(L_f/d_f)/2$, and $\tilde{\delta} \equiv \delta/(L_f/2)$. $\tilde{\delta}^* \equiv (2\tau/(1+\eta)E_f)(L_f/d_f)$ corresponds to the maximum attainable value of δ_0 (normalized by $L_f/2$) for the fiber with the longest embedment length of $L_f/2$. The snubbing factor g in (4) is defined in terms of the snubbing coefficient f:

$$g \equiv \frac{2}{4+f^2}(1 + e^{\pi f/2}) \quad \ldots\ldots\ldots\ldots\ldots\ldots\ldots\ldots\ldots\ldots (5)$$

In (4), higher-order terms of $(\tilde{\delta}/\tilde{\delta}^*)$ have been dropped. The full expression and a detailed derivation of (4) and its postpeak tension-softening counterpart, together with comparisons with experimental data, is given in Li (1992). [In Li (1992) the analysis was carried out for the case where matrix stiffness is large compared with fiber stiffness and/or where the fiber volume fraction is low, so that $\eta \to 0$. By observation, all results from that analysis can be carried over to the present more general case simply by multiplying the fiber modulus by the factor $(1+\eta)$]. σ_0 may be interpreted as the maximum bridging stress when the snubbing mechanism is inactive (i.e., $f = 0$, or $g = 1$). Eq. (4) is used to compute the prepeak part of the σ_B-δ curve, shown in Fig. 1, for various snubbing coefficients. In general, the peaks of the σ_B-δ curves occur at δ just less than δ^*.

Energy is absorbed in the frictional debonding process. This part of the fracture energy G_f may be estimated by integrating the prepeak stress-crack opening curve [(4)] with respect to δ up to δ^*. The result is

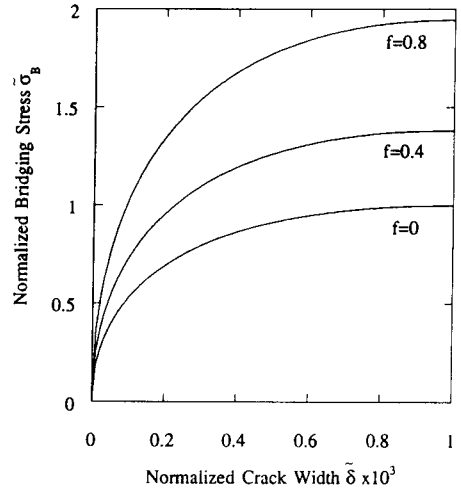

FIG. 1. Prepeak Fiber-Bridging Stress versus Crack-Opening Relationship

$$G_r = \frac{5}{24} g\tau V_f d_f \left(\frac{L_f}{d_f}\right)^2 \tilde{\delta}^* \quad \ldots\ldots (6)$$

First-Crack Strength

The first-crack strength represents the applied tensile stress at which a matrix crack spreads throughout a cross section of a composite loaded in tension. In a fiber composite, propagation of a matrix crack is resisted by matrix toughness as well as by bridging fibers. Aveston et al. (1971) considered the energy balance in the propagation of a matrix crack in an aligned continuous fiber reinforced composite under the steady-state condition. This approach yields a lower bound of the composite critical strain. (The phrase *steady-state cracking* is used to describe the spreading of a crack under nominally constant applied load.) They showed that such a critical strain can be several times higher than the matrix strain, and could be achieved with small-radius fibers held in the matrix by frictional bond. Aveston and Kelly (1973) considered the case where the fibers are elastically bonded to the matrix. Budiansky et al. (1986) extended their analyses to the intermediate case between full frictional sliding and no sliding, as well as slightly elastically bonded but debonding fibers. To include presteady-state cracking when the first-crack strength must depend on matrix flaw size, Marshall et al. (1985) and Marshall and Cox (1987) reanalyzed the problem based on balancing of the stress-intensity factor due to loading, bridging, and matrix-toughness resistance. A similar technique was employed by Li and Liang (1986) in deriving the R-curve behavior associated with the bridging-zone growth in tension-softening materials. To include matrix tension-softening effect, Shah (1990) adopted a similar approach that directly includes experimentally measured σ_B-δ relations for specific fiber/matrix systems. In the last two references, steady-state cracking was not considered. The aforementioned studies were all conducted for aligned, continuous fiber-reinforced composites. Leung and Li (1989) extended the analyses of Marshall and coworkers to discontinuous aligned-fiber systems.

The present analysis of first-crack strength in discontinuous random flexible fiber composite is based on the fracture mechanics approach whereby the bridging action of fibers is treated as cohesive traction acting across the crack flanks. Balancing of the combined stress-intensity factor due to applied remote loading K_L and that due to fiber bridging behind the crack tip K_B, with the crack-tip–fracture toughness K_{tip} requires:

$$K_L + K_B = K_{tip} \quad \ldots\ldots (7)$$

For small fiber-volume fraction K_{tip} can be taken to be simply the matrix toughness K_m. Otherwise, following Marshall et al. (1985), $K_{tip} = (E_c/E_m)K_m$, since the stress intensity factor scales directly with stress. E_c = the composite elastic modulus and E_m, K_m = the matrix modulus and fracture toughness, respectively.

For a penny-shaped crack of radius c, the normalized stress-intensity factor due to ambient tensile loading σ is given by

$$\tilde{K}_L \equiv \frac{K_L}{\sigma_0\sqrt{c_0}} = 2\sqrt{\frac{\tilde{c}}{\pi}}\,\tilde{\sigma} \quad \ldots\ldots (8)$$

where

$$c_0 \equiv \left(\frac{L_f E_c}{2K_{tip}}\right)^2 \frac{\pi}{16(1-\nu^2)^2} \quad \ldots\ldots (9)$$

serves as a convenient nondimensioning factor for the crack radius such that the normalized crack radius $\tilde{c} \equiv c/c_0$. In (9), ν = the composite Poisson's ratio.

The normalized stress-intensity factor due to fiber bridging may be obtained by integrating the solution for a penny-shape crack loaded by concentric distributed pressure at r [see, e.g., Tada et al. (1973)] over the crack plane

$$\tilde{K}_B \equiv \frac{K_B}{\sigma_0\sqrt{c_0}} = -2\sqrt{\frac{\tilde{c}}{\pi}}\int_0^1 \tilde{\sigma}_B(\tilde{\delta})\frac{RdR}{\sqrt{1-R^2}} \quad \ldots\ldots (10)$$

where $R \equiv r/c_0$. The negative sign in (10) is due to the crack-closing effect of the fiber-bridging stress. In general, the crack opening $\tilde{\delta}$ is not known a priori as a function of position R, and evaluation of K_B typically requires an iterative process. For simplicity, the crack profile is assumed to take on the same parabolic shape as if the bridging stresses on the crack flanks are uniform. (This assumption holds so long as steady-state cracking has not been reached; see discussion to follow.) Based on numerical analysis, Marshall et al. (1985) showed that this simplification leads to an approximately 20% overestimation of the first-crack strength for continuous fiber composites. For the parabolic-shape crack, the normalized crack opening is given by:

$$\tilde{\delta} = \sqrt{\tilde{c}(1-R^2)} \quad \ldots\ldots (11)$$

The first-crack strength σ_{fc} may be obtained when (7) is met, and making use of (4), (8), (10), and (11):

$$\frac{\tilde{\sigma}_{fc}}{g} = \frac{\sqrt{\pi}}{2}\frac{\tilde{K}}{\tilde{c}} + \left(\frac{4}{3}\sqrt{\tilde{c}} - \frac{1}{2}\tilde{c}\right) \quad \ldots\ldots (12)$$

where $\tilde{K} \equiv (K_{tip}/\sigma_0\sqrt{c_0})/g\tilde{\delta}^*$, $\tilde{c} \equiv \sqrt{\tilde{c}}/\tilde{\delta}^*$. The first term on the right-hand side of (12) is the matrix-toughness–induced strength. The second term in brackets represents the contribution to composite strength due to fiber bridging. Eq. (12) for the first-crack strength is valid as long as the crack shape remains parabolic as the bridging zone grows. In reality the fibers in the center of the crack, where the crack opening is maximum, would be pulled out with decreasing load subsequent to full frictional debonding along their lengths after a certain amount of crack growth. If, however, the rising bridging force during debonding reaches the magnitude of the applied remote load, the crack flanks will flatten out (Marshall and Cox 1987) and the crack front can continue to propagate at constant load, i.e., a state of steady crack extension has been created.

Steady-State Cracking

The discussion just presented suggests that steady-state cracking occurs under two conditions: (1) The stress at the midpoint of the crack σ_m must equal the first crack strength σ_{fc}; and (2) the crack-opening displacement at the midpoint of the crack δ_m must be less than the displacement δ_p corresponding to the maxima of the bridging stress as expressed in (4).

The first condition implies that the intercept of the $\tilde{\sigma}_{fc}(\tilde{c})$ and the $\tilde{\sigma}_m(\tilde{c})$ curves determines the normalized crack size $\tilde{c}_s$ at which steady-state cracking begins. That is, when

$$\tilde{\sigma}_m[\equiv\tilde{\sigma}_B(\tilde{\delta} = \tilde{\delta}_m \equiv \sqrt{\tilde{c}})] = \tilde{\sigma}_{fc} \quad \ldots\ldots\ldots\ldots\ldots\ldots\ldots\ldots\ldots\ldots (13)$$

then using (4) and (12) in (13), $\tilde{c}_s$ is defined by

$$\tilde{K} = \frac{2}{\sqrt{\pi}}\,\tilde{c}_s\left(\frac{2}{3}\sqrt{\tilde{c}_s} - \frac{1}{2}\,\tilde{c}_s\right) \qquad (0 \le \tilde{c}_s \le 1) \quad \ldots\ldots\ldots\ldots\ldots\ldots (14)$$

At this stage, the crack propagates at essentially no further increase in load and a steady-state cracking phenomenon results. The load at steady state is often called the steady-state first-crack strength $\tilde{\sigma}_{ss}$.

The second condition implies a limiting value of $\tilde{K} = \tilde{K}_{crit}$ beyond which no steady-state cracking can take place. This occurs at $\tilde{c}_s = \tilde{c}_p = 1$. From (14), $\tilde{K}_{crit}$ is found to be $1/(3\sqrt{\pi}) \approx 0.188$. Fig. 2 illustrates the two conditions of steady-state cracking schematically.

For a composite with a $\tilde{K}$ larger than $\tilde{K}_{crit}$, the material will fall immediately at the first-crack strength, with fiber pullout spreading from the center to the outer periphery of the crack. The failure strength in this case will be determined by (12) and depends on the flaw size $\tilde{c}$. Although toughened by the presence of fibers, the composite remains essentially notch-sensitive as in a Griffith material. For a composite with a $\tilde{K}$ smaller than $\tilde{K}_{crit}$, the material will fail at the steady-state strength $\tilde{\sigma}_{ss}$, and becomes independent of flaw sizes, as long as $\tilde{c}$ is larger than $\tilde{c}_s$, i.e., the composite becomes notch-insensitive. These ideas are illustrated for a range of $\tilde{K}$ values in Fig. 3, which shows the first-crack strength plotted as a function of flaw size, based on (12) and (14). Fig. 4 shows the corresponding value of $\tilde{c}_s$ as a function of $\tilde{K}$. Note that $\tilde{c}_s$ approaches infinity as $\tilde{K}$ approaches $\tilde{K}_{crit}$.

Because of the important role that $\tilde{K}$ plays in governing composite behavior, it is useful to examine in a bit more detail the physical meaning of this parameter. With the help of (6), it can be shown that $\tilde{K}$ can be rewritten as a ratio of crack-tip fracture-energy–absorption rate G_{tip} to the

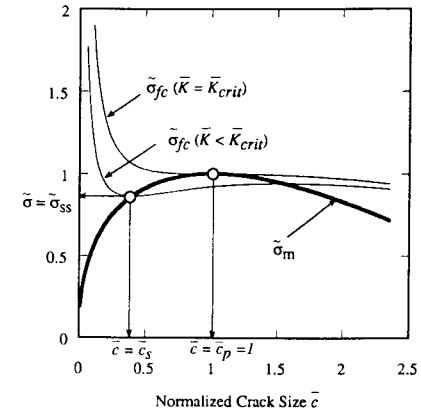

FIG. 2. First-Crack Strength and Bridging Stress at Midcrack Position; Conditions for Steady-State Cracking Requires these Curves to Meet, i.e., $\tilde{K} < \tilde{K}_{crit}$

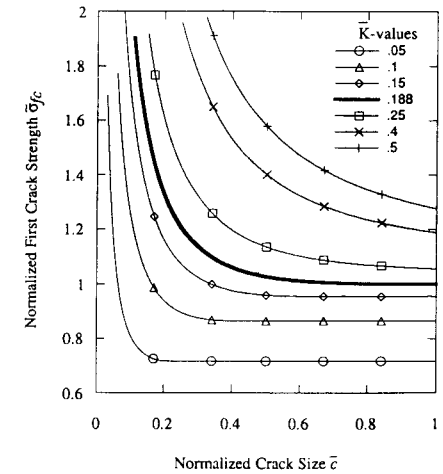

FIG. 3. First-Crack Strength Decay with Flaw Size; For High $\tilde{K}$ Values (above Solid Black Line), Material Remains Notch-Sensitive; For Low $\tilde{K}$ Values (below Solid Black Line), Material Becomes Notch-Insensitive in Plateau Region

energy-absorption rate in the fiber-bridging zone G_r behind the crack front, whence:

$$\tilde{K} = \frac{10}{3\sqrt{\pi}}\left(\frac{G_{tip}}{G_r}\right) \quad \ldots\ldots\ldots\ldots\ldots\ldots\ldots\ldots\ldots\ldots\ldots\ldots\ldots\ldots\ldots\ldots (15)$$

This new interpretation of $\tilde{K}$ emphasizes the importance of fiber reinforcement in achieving steady-state cracking (and the potential of subsequent multiple cracking, to be discussed). Specifically, G_r scales linearly with fiber-volume fraction and the snubbing factor g, to the square of the bond strength, and to the third power of fiber aspect ratio. Increasing values of these

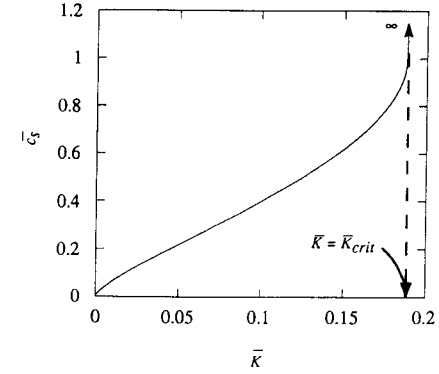

FIG. 4. Transition Value of Crack Size When Crack Begins to Flatten

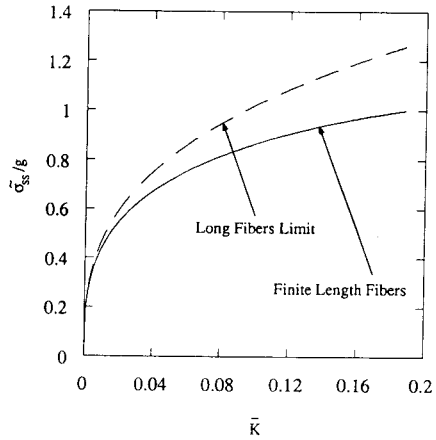

FIG. 5. Comparison of Predicted Steady-State Crack Strength Based on Finite [(14) and (18)] and Long-Fiber Limit [(19)] Considerations

parameters will therefore lead to a reduction in $\tilde{K}$ and enhance steady-state cracking.

The interpretation of $\tilde{K}$ in (15) affords additional insight into its critical value $\tilde{K}_{crit}$. The requirement for steady-state cracking may now be rewritten in the form

$$G_r \geq 10 G_{tip} \quad \ldots\ldots (16)$$

or, using (6)

$$V_f \geq V_f^{crit} \equiv \frac{48 G_{tip}}{g\tau d_f \left(\frac{L_f}{d_f}\right)^2 \tilde{\delta}^*} \quad \ldots\ldots (17)$$

Eqs. (16) and (17) define the minimum bridging fracture energy and fiber-volume fraction necessary for achieving steady-state cracking. For some typical FRCs, with parametric values given in Table 1, the critical fiber volume fractions are found to be in the range of 0.5 to 4%. Eq. (17) suggests

TABLE 1. Critical Fiber-Volume Fraction for Various Fiber Types in Ordinary Portland Cement Matrix

Fiber Type (1)	E_f (GPa) (2)	τ (MPa) (3)	d_f (μm) (4)	L_f/d_f (5)	$V_{f,crit}$ (%) (6)
Steel	200	7	250	100	3.6
Glass	80	0.3	12	3,000	0.4
Carbon (pitch)	40	8	15	200	0.6
PP	6	0.7	70	186	2.9

Note: $E_m = 20$ GPa; $G_m = 100 \times 10^{-6}$ MPa-m.

that as the fracture energy of the matrix increases, the fiber-volume fraction must correspondingly increase in order to maintain steady-state cracking and keep the composite from becoming notch-sensitive. It is also clear that smaller fiber diameter, such as that afforded by carbon or glass, makes it easier to achieve steady-state cracking with smaller fiber-volume fraction required.

The steady-state crack strength may be evaluated from (4) and (11), and identifying $\bar{c}$ as $\bar{c}_s$, leads to

$$\tilde{\sigma}_{ss} = g(2\sqrt{\bar{c}_s} - \bar{c}_s) \quad \ldots\ldots (18)$$

Eqs. (14) and (18) form a pair of parametric equations in $\bar{c}_s$. Fig. 5 shows the relation between $\tilde{\sigma}_{ss}$ and $\tilde{K}$. The critical strain ε_{ss} may then be calculated from σ_{ss}/E_c, assuming a linear stress-strain relationship up to steady-state cracking. In the limit when the fiber aspect ratio is large, we expect to recover the results of the classical ACK theory (Aveston et al. 1971) modified for the effect of fiber randomness. This is indeed the case when we drop the higher-order terms of $\bar{c}_s$ inside the parentheses of (14) and (18), so that

$$\tilde{\sigma}_{ss} = g(6\sqrt{\pi}\tilde{K})^{1/3} \quad \ldots\ldots (19)$$

and hence

$$\varepsilon_{ss} = \left[\frac{3g^2 V_f^2 \tau G_m E_f}{E_c E_m^2 r_f V_m}\right]^{1/3} \quad \ldots\ldots (20)$$

where r_f = the fiber radius, and the matrix fracture energy G_m is related to K_{tip} via

$$\frac{G_m}{E_m} = \frac{1}{E_c}\left(\frac{(1-\nu^2)K_{tip}^2}{E_c}\right) \quad \ldots\ldots (21)$$

The ACK theory predicts a critical strain value of

$$\varepsilon_{mu} = \left[\frac{12 v_f^2 \tau \gamma_m E_f}{E_c E_m^2 r_f V_m}\right]^{1/3} \quad \ldots\ldots (22)$$

Eqs. (20) and (22) are equivalent if we further recognize that $G_m = 2\gamma_m$, where γ_m = the surface energy. Further, a factor of 2 difference inside the square bracket may be expected since (20) is derived for a 3-D random fiber composite while (22) is for the case of continuous aligned-fiber reinforce-

ment (Aveston et al. 1971, 1974). When the snubbing mechanism is inoperative as in the case of aligned fibers, g = unity.

The steady-state cracking stress for the long-fiber limit [(19)] is also shown in Fig. 5. As expected, the difference (dashed line, in percentages) between this limiting case and the general case of arbitrary fiber length increases with $\bar{K}$. For short-fiber systems with $\bar{K}$ larger than 0.05, the error in using (19) exceeds 10%, suggesting that (14) and (18) should be used instead.

Fig. 6 illustrates the influence of fiber diameter on the first-crack strength. Parametric values of steel fibers of fixed length have been assumed. This figure clearly demonstrates the advantage of using fibers with smaller diameters in producing a composite with high first-crack strength. Critical fiber-volume fractions in each case are also indicated, and shown to decrease with fiber diameter.

Multiple Cracking

For $\bar{K} \leq \bar{K}_{crit}$, steady-state cracking is guaranteed. After a first crack is formed, two scenarios are possible. The fibers bridging across the crack may not be able to sustain the total load: the sum of the initial load carried by the fibers just prior to first crack, and the additional load shed by the matrix. This will lead to fiber pullout. If, however, the fibers were able to sustain the total load, the fibers would transfer the load back to the matrix through interfacial shear, eventually leading to the formation of another crack. This process then repeats itself until a set of periodic subparallel cracks are formed. Subsequently, additional load could be applied until the postcrack strength σ_0 (the maximum value of the σ_B-δ curve) is reached.

The presence or absence of multiple cracking is determined by the first-crack strength, which in turn is dependent on the crack size (see Fig. 2). The condition for multiple cracking therefore becomes

$$\sigma_{fc}(c) \leq g\sigma_0 \quad \ldots\ldots (23a)$$

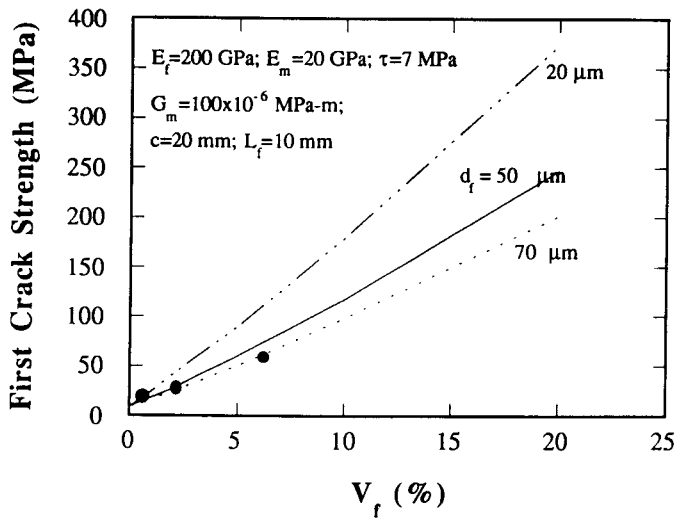

FIG. 6. Dependence of First-Crack Strength on Fiber Diameter; for Each Fiber Diameter, Critical Fiber-Volume Fraction is Marked

or

$$\frac{\bar{\sigma}_{fc}(\bar{c})}{g} \leq 1 \quad \ldots\ldots (23b)$$

which then defines a minimum normalized crack size $\bar{c}_{mc}$ for which multiple cracking would occur. Using (12) and (23) in the upper limit:

$$\frac{\sqrt{\pi}}{2}\frac{\bar{K}}{\bar{c}_{mc}} + \left(\frac{4}{3}\sqrt{\bar{c}_{mc}} - \frac{1}{2}\bar{c}_{mc}\right) = 1 \quad \ldots\ldots (24)$$

The complete criteria for multiple cracking in a discontinuous random-fiber composite then becomes

$$\bar{K} \leq \bar{K}_{crit} \quad \ldots\ldots (25a)$$

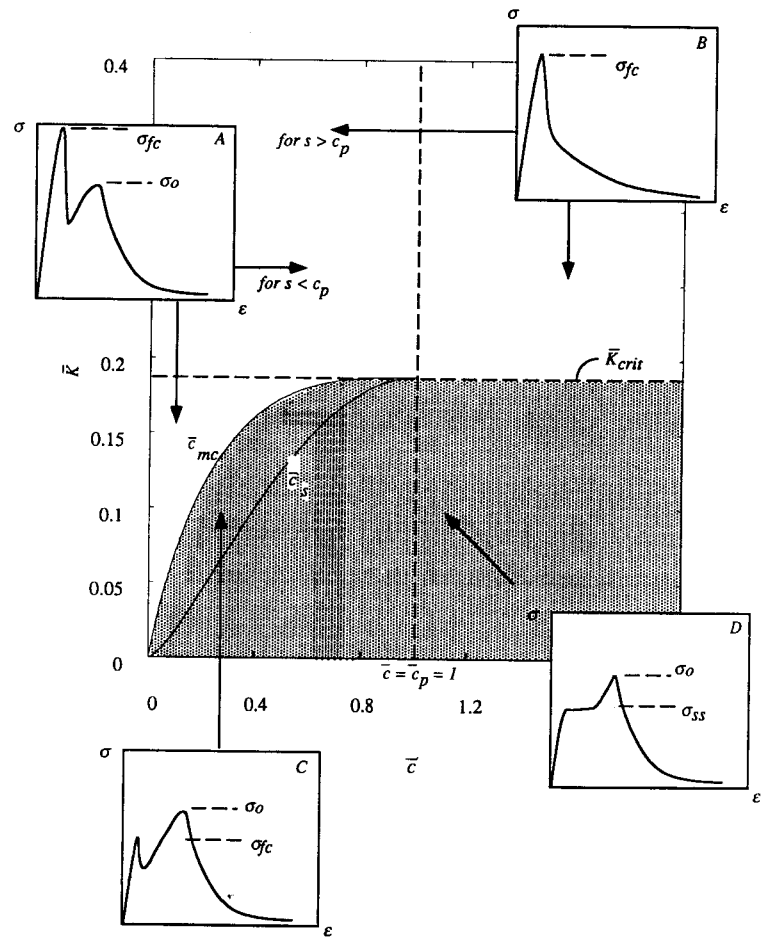

FIG. 7. Failure-Mechanism Map; Shaded Region (Low $\bar{K}$-high $\bar{c}$ Combination) Gives Pseudostrain-Hardening Tensile Behavior

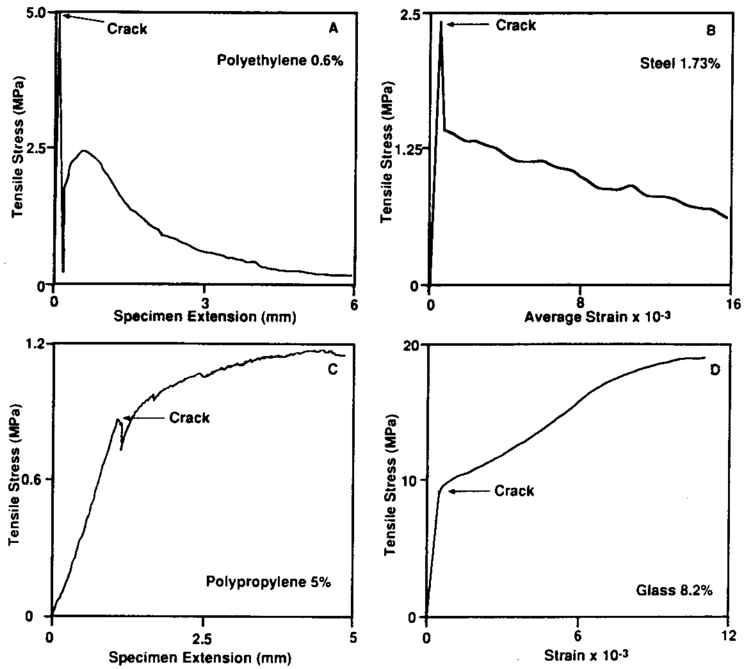

FIG. 8. Experimental Stress-Deformation Curves for Various Cementitious Composites Showing Different Modes of Failure Corresponding to those Indicated in Different Regions of Failure-Mechanism Map of Fig. 7: (*a*) Spectra Polyethylene FRC [after Green (1989)]; (*b*) Steel FRC [after Shah et al. (1979)]; (c) Polypropylene FRC [after Bagott (1983)]; (*d*) Glass FRC [after Ali et al. (1975)]

and

$$\bar{c}_{mc} \leq \bar{c} \qquad (25b)$$

These conditions for multiple cracking, together with that for steady-state cracking, are conveniently summarized in the failure mechanism $\bar{K}$-$\bar{c}$ map shown in Fig. 7. The expected load-deformation behavior for various $\bar{K}$-$\bar{c}$ combinations are also schematically illustrated in the inserts of Fig. 7. Below the $\bar{K}_{crit}$ line, $\bar{K}$-$\bar{c}$ combinations to the right of the $\bar{c}_s$ curve will lead to steady-state cracking at constant stress σ_{SS} followed by multiple cracking until the applied load has risen to σ_0. For composites with $\bar{K}$-$\bar{c}$ combinations to the left of the $\bar{c}_{mc}$ curve, the first-cracking strength can be much higher than σ_0, but first crack will be followed by a sudden drop in load-bearing capacity, with a subsequent rise to σ_0 before final softening as a single crack enlarges. For composites with $\bar{K}$-$\bar{c}$ combinations that fall between the $\bar{c}_{mc}$ and $\bar{c}_s$ curves, multiple cracking could be accompanied by an initial load drop, then by a rising load.

Above the $\bar{K}_{crit}$ line, no steady-state or multiple cracking can occur. The material will fail catastrophically like a Griffith-type material, even though the first-crack strength and the fracture toughness of the composite would still be higher than that of the matrix material. For $\bar{c} \leq \bar{c}_p$ ($\bar{c}_p = 1$), if the specimen cross-sectional size s is small, there is a possibility that by the time the first crack spread to the edge of the specimen, the crack opening in the

TABLE 2. Estimated $\bar{K}$-$\bar{c}$ and Expected Tensile Failure Modes for Four FRCs

Fiber (1)	Matrix (2)	E_m (GPa) (3)	E_f (GPa) (4)	τ[a] (MPa) (5)	$G_m \times 10^{-6}$[a] (MPa-m) (6)	K_m[a] (MPa-m$^{1/2}$) (7)	c[b] (mm) (8)	V_f (%) (9)	$\bar{K}$ (10)	$\bar{c}$ (11)	$\bar{c}_s$ (12)	$\bar{c}_{mc}$ (13)	$s/2$ (mm) (14)	c_p (mm) (15)	Failure mode (16)
Glass	OPC paste	26	76	0.3	1.5	0.2	6	8.2	0.00027	0.0055	0.0053	0.001	—	—	D
PP	Lightweight mortar	2.2	2	0.5	4.5	0.1	6	5.0	0.0016	0.018	0.02	0.011	—	—	C
Spectra	HS concrete	*20	120	1.0	20.0	0.63	20	0.6	0.65	0.38	—	—	25	246	A
Steel	OPC mortar	*20	200	2.5	18.0	0.6	30	1.73	0.91	0.65	—	—	100	71	B

[a]Assumed values.
[b]Assumed effective flaw size.

middle would still be smaller than δ^*, so that a small rise in load is possible prior to full crack separation. This happens if $s/2 \leq c_0\delta^{*2}$. In all cases an R-curve behavior may be expected due to fiber pullout.

The various types of tensile failure behavior depicted in Fig. 7 have been reported in the literature. Some examples are given in Fig. 8 for steel-fiber–reinforced concrete (Shah et al. 1979), Spectra (a high-modulus polyethylene) fiber-reinforced high-strength concrete (Green 1989), polypropylene fiber-reinforced mortar (Baggot 1983) and glass-fiber–reinforced ordinary portland cement (Ali et al. 1975). Information on fiber and matrix properties can be found in Table 2. Computed values of $\bar{K}$, $\bar{c}$, $\bar{c}_{mc}$, $\bar{c}_s$, and c_p, as well as the expected tensile-failure mode for each material are also given in Table 2. Several parameters including the matrix toughness or fracture energy, the bond strength, and the initial flaw size are not given in the references and have to be estimated. Constraints for these estimates are provided by the measured matrix tensile strength and the composite first-crack strength for the given fiber-volume fraction. In the case of Spectra FRC, the reported low-composite strength (lower than the matrix strength) demands a very large "effective" flaw size, suggesting that poor workability led to large flaw size, with potential crack-crack interaction effect.

For Spectra FRC, the $\bar{K}$ value of 0.65 is higher than the $\bar{K}_{\text{crit}}$ value of 0.188. This implies that the composite will not be adequately reinforced to exhibit steady-state and multiple cracking. The specimen half-width $s/2$ (25 mm) is smaller than the computed c_p value (246 mm). From Fig. 7, this material is expected to fail in mode A. For the steel FRC, the $\bar{K}$ value of 0.91 is again larger than $\bar{K}_{\text{crit}}$. However, the specimen half-width $s/2$ (100 mm) is higher than the calculated c_p (71 mm) for this material, so that according to Fig. 7, the material is expected to fail in mode B. For the polypropylene FRC, the $\bar{K}$ value of 0.0016 falls below $\bar{K}_{\text{crit}}$, and therefore have the potential to undergo steady-state and multiple cracking. However, its $\bar{c}$ value (0.018) falls between $\bar{c}_{mc}$ (0.011) and $\bar{c}_s$ (0.02), so that an initial load drop at first cracking is expected prior to multiple cracking. This corresponds to failure mode C, according to Fig. 7. For the glass FRC, the $\bar{K}$ value of 0.00027 falls below $\bar{K}_{\text{crit}}$, and its $\bar{c}$ value of 0.0055 is just higher than the $\bar{c}_s$ value of 0.0053. Hence this material should undergo steady-state and multiple cracking, with a failure mode of D.

Conclusions

The conditions for steady-state and multiple cracking for a 3-D randomly distributed discontinuous fiber-reinforced composite have been analyzed. It is found that a single nondimensional parameter, interpretable as the ratio of crack tip to crack-bridging fracture energy, determines whether steady-state cracking can be achieved. This leads to a minimum or critical fiber-volume fraction [(17)], expressible in terms of micromechanical parameters, for occurrence of steady-state cracking. Since steady-state cracking is clearly a precondition for pseudostrain hardening, it is now possible to consider engineering of cementitious composites using (17) in order to attain ductile tensile behavior. For example, the tailoring of τ/E_f, L_f/d_f, and $G_m/g\tau d_f$ may lead to reduced critical fiber-volume fraction in order to enhance steady-state cracking while reducing cost (assuming the normal situation of fiber cost higher than matrix cost) and improving processing ease. More specifically, doubling the aspect ratio through L_f implies a significant reduction of 87.5% of fibers needed to achieve the same effect. Furthermore, if c_s is

made smaller than fabrication flaw sizes, then a notch-insensitive behavior sets in, resulting in a composite with high reliability.

Steady-state cracking is accompanied by a higher first-cracking strength and strain. It is shown in this paper that these quantities can again be related to microstructural parameters, which could be tailored for pseudostrain-hardening enhancement. Although the failure strength is less than that for a continuous system as expected, the present study indicates that its magnitude can be enhanced by a snubbing effect associated with inclined bridging (flexible) fibers.

For multiple cracking to occur, the present analysis reveals that a $\bar{c}_{mc}$, defined by (24), must be smaller than the fabrication flaw size. Because $\bar{c}_{mc}$ is relatable to $\bar{K}$ (see Fig. 7), (24) may be used to engineer a composite containing discontinuous fibers for multiple cracking. Furthermore, it is found that the $\bar{K}$-$\bar{c}$ combination determines the various types of tensile failure behavior, all of which have been reported in the literature. Because the $\bar{K}$-$\bar{c}$ mechanism map (Fig. 7) is expressed in nondimensional form, it can be utilized for pseudostrain-hardening design of any discontinuous random-fiber–reinforced composites, so long as the essential micromechanical failure mechanisms are well described by those assumed in the present model.

Finally, it should be noted that all calculations performed in this paper are based on a composite modulus E_c that relates to the fiber and matrix moduli, and fiber-volume fraction by the classical rule of mixture. This simple relation gives an upper bound to the actual composite modulus, which is expected to depend on fiber-aspect ratio as well. More accurate (but more complicated) expressions of E_c can be found in Tandon and Weng (1986) and Wakashima and Tsukamoto (1991). Except for high fiber-volume fraction (more than 10%) the errors introduced (in, e.g., σ_{fc} and V_f^{crit}) have been found to be within 10%.

Appendix I: P-δ Relation for Bridging Fiber

The P-δ relation may be obtained from a shear-lag analysis as carried out in Leung and Li (1991a). For the fiber displacement (at the location of the matrix-crack plane) relative to the matrix deformation, they derived the following relationship between the fiber stress σ_p and the displacement u at the matrix-crack plane:

$$\frac{u}{r_f} = \frac{\tau_s \log\left(\frac{R^*}{r_f}\right)}{G} + \left[\frac{\sigma_p}{E_f}\right]\left(\frac{L_d}{r_f}\right) - \frac{\tau E_c \left(\frac{L_d}{r_f}\right)^2}{E_f V_m E_m} \quad \text{..... (26)}$$

where τ_s = the elastic-bond strength; r_f = the fiber radius; R^* = effective radius of the matrix cylinder containing the fiber; G = the matrix shear modulus; σ_p ($\equiv P/\pi r_f^2$) = the fiber traction at the location of the matrix-crack plane; and L_d = the debond length. The other terms are already defined in the text. The first term in (26) originates from elastic-stress transfer of the bonded fiber segment, and is generally small compared to the other terms in (26). Ignoring this term leads to

$$\frac{u}{r_f} = \left(\frac{\sigma_p}{E_f}\right)\left(\frac{L_d}{r_f}\right) - \frac{\tau E_c \left(\frac{L_d}{r_f}\right)^2}{E_f V_m E_m} \quad \text{..... (27)}$$

Leung and Li also derived the fiber traction as a function of debond length:

$$\sigma_p = \frac{\left[2\left(\frac{L_d}{r_f}\right)\tau \cosh Z + 2\left(\frac{\tau_s}{\rho}\right)\sinh Z\right]}{(1-\alpha)\cosh Z + \alpha} \quad \ldots\ldots (28)$$

where $Z = \rho(L_f - L_d)/r_f$; $\alpha = V_f E_f/E_c$; and $\rho^2 = 2GE_c/[V_m E_m E_f \log(R^*/r_f)]$.

In the main body of this paper we have assumed weak adhesion between the fiber and the matrix, so that $\tau_s = \tau$. The first term in (28) is much larger than the second provided that

$$\left(\frac{L_d}{r_f}\right) >> \frac{1}{\rho} \quad \ldots\ldots (29)$$

which is generally satisfied as soon as the debond length is larger than about 10 fiber diameters. Using these assumptions and for moderately small fiber-volume fraction so that $\alpha << 1$, (28) may be simplified to the following:

$$\sigma_p = \frac{2\tau\left(\frac{L_d}{r_f}\right)}{(1-\alpha)} \quad \ldots\ldots (30)$$

(27) and (30) form a pair of equations where P and u are related parametrically through the debond length L_d. When combined, they form:

$$\sigma_p = \sqrt{4\left(\frac{u}{r_f}\right)(1+\eta)\tau E_f} \quad \ldots\ldots (31)$$

The fiber-bridging force is then given by

$$P(u) = \pi\sqrt{\frac{(1+\eta)E_f d_f^3 \tau u}{2}} \quad \ldots\ldots (32)$$

Eq. (32) is identical to a result derived by Marshall et al. (1985) using a different approach. The assumptions that went into deriving (32) are consistent with that used by Aveston et al. (1971), who obtained the critical composite strain given in (22). If elastic-stress transfer needs to be accounted for, or that the fiber/matrix adhesion is strong enough to raise τ_s much above τ, or that high fiber-volume fraction and/or stiffness is used, (26) and (28) provide a more accurate description of the relationship between P and u. A modified version of (28) (Leung and Li 1991) accounts for the possibility of debonding occurring at the embedded fiber end after some debonding from the crack-plane end. However, an iterative procedure is needed to obtain the P-u relationship for the two-way debonding process, too complicated to use for the purpose of this paper. Moreover, Leung and Li showed that for weakly bonded fibers, the one-way debonding theory adopted in the present work is accurate up to 90% of the peak pull-out load.

For a fiber bridging a matrix crack, debonding occurs on embedded segments on both sides of the crack so that the crack opening $\delta = 2u$. The required $P(\delta)$ relation is then given by:

$$P(\delta) = \frac{\pi}{2}\sqrt{(1+\eta)E_f d_f^3 \tau \delta} \quad \ldots\ldots (33)$$

When a fiber is making an angle θ to the normal of a crack, it can be shown that the fiber-bridging force for a certain crack opening δ is given by:

$$P(\delta) = \frac{\frac{\pi}{2}\sqrt{(1+\eta)E_f d_f^3 \tau \delta}}{1+\eta(1-e^{f\theta}\cos\theta)} e^{f\theta} \quad \ldots\ldots (34)$$

where the exponential function $e^{f\theta}$ accounts for the snubbing effect while the term $\eta(1 - e^{f\theta}\cos\theta)$ in the denominator accounts for matrix deformation due to the force acting on the matrix at the exit point of the fiber (where snubbing occurs). If (34) is used together with (3) to compute the composite $\sigma_B - \delta$ relation, a simple analytical expression [such as (4)] can no longer be obtained. The first-crack strength as well as the criteria for steady-state cracking and multiple cracking are then no longer expressible in simple forms that provide insights into the relative effects of various parameters on composite behavior. A simplified form of (34) is therefore desirable. For most composite systems with flexible fibers, the value of η is small (usually less than 0.1). The snubbing coefficient f also rarely exceeds unity. For such cases, neglecting the term $\eta(1 - e^{f\theta}\cos\theta)$ will only introduce a slight error of less than 5% to the composite $\sigma_B - \delta$ relation. Therefore, for the analyses in the text, we drop the denominator in (34) to obtain:

$$P(\delta) = \frac{\pi}{2}\sqrt{(1+\eta)E_f d_f^3 \tau \delta}\, e^{f\theta} \quad \ldots\ldots (35)$$

For high fiber-volume fraction, say 10%, coupled with high value of f, say 1, (34) must be used in place of (35).

Acknowledgments

Research at the Advanced Civil Engineering Materials Research Laboratory has been supported by a research grant from the National Science Foundation (program manager: Dr. K. Chong) to the University of Michigan, Ann Arbor. Helpful discussions with H. C. Wu and Y. W. Chan are gratefully acknowledged.

Appendix II. References

Ali, M. A., Majumdar, A. J., and Singh, B. (1975). "Properties of glass fiber cement—the effect of fiber length and content." *J. Mater. Sci.*, 10, 1732–1740.

Aveston, J., and Kelly, A. (1973). "Theory of multiple fracture of fibrous composites." *J. Mater. Sci.*, 8, 352–362.

Aveston, J., Cooper, G. A., and Kelly, A. (1971). "Single and multiple fracture." *The properties of fiber composites*, Science and Technology Press Ltd., England, 15–24.

Aveston, J., Mercer, R. A., and Sillwood, J. M. (1974). "Fiber reinforced cements—scientific foundations for specifications." *Composites standards testing and design, Conf. Proc. National Physical Laboratory*, IPC Science and Technology Press, Guildford, United Kingdom, 93–103.

Baggott, R. (1983). "Polypropylene fiber reinforcement of lightweight cementitious matrices." *Int. J. Cem. Compos. Lightweight Concr.*, 5(2), 105–114.

Brandt, A. M. (1985). "On the optimal direction of short metal fibers in brittle matrix composites." *J. Mater. Sci.*, 20, 3831–3841.
Broek, D. (1986). *Elementary engineering fracture mechanics*, 4th Ed., Martinus Nijhoff Publishers, Dordrecht, the Netherlands.
Budiansky, B., Hutchinson, J., and Evans, A. G. (1986). "Matrix fracture in fiber-reinforced ceramics." *J. Mech. and Physics of Solids*, 34(2), 167–189.
Green, E. (1989). "Behavior of high strength fiber reinforced concrete," MS thesis, Massachusetts Institute of Technology, Cambridge, Mass.
Leung, C. K., and Li, V. C. (1989). "First-cracking strength of short fiber-reinforced ceramics." *Ceram. Eng. Sci. Proc.*, 9/10, 1164–1178.
Leung, C. K., and Li, V. C. (1991). "New strength based model for the debonding of discontinuous fibers in an elastic matrix." *J. Mater. Sci.*, 26, 5996–6010.
Leung, C. K., and Li, V. C. (1992). "Effects of fiber inclination on crack bridging stresses in fiber reinforced brittle matrix composites." *J. Mech. and Physics of Solids.*
Li, V. C. (1992). "Post-crack scaling relations for fiber reinforced cementitious composites." *J. Mater. in Civ. Engrg.*, ASCE, 4(1), 41–57.
Li, V. C., and Liang, E. (1986). "Fracture processes in concrete and fibre-reinforced cementitious composites." *J. Engrg. Mech.*, ASCE, 122(6), 566–586.
Li, V. C., Wang, Y., and Backer, S. (1990). "Effect of inclining angle, bundling, and surface treatment on synthetic fiber pull-out from a cement matrix." *Composites*, 21(2), 132–140.
Li, V. C., Wang, Y., and Backer, S. (1991). "A micromechanical model of tension-softening and bridging toughening of short random fiber reinforced brittle matrix composites. *J. Mech. and Physics of Solids*, 39(5), 607–625.
Marshall, D. B., and Cox, B. N. (1987). "Tensile fracture of brittle matrix composites: influence of fiber strength." *Acta Metall.*, 35(11), 2607–2617.
Marshall, D. B., Cox, B. N., and Evans, A. G. (1985). "The mechanics of matrix cracking in brittle matrix fiber composites." *Acta Metall.*, 3(11), 2013–21.
Morton, J., and Grove, G. W. (1976). "The effect of metal wires on the fracture of a brittle matrix composite." *J. Mater. Sci.*, 11, 617–622.
Shah, S. P. (1990). "Toughening of quasi-brittle materials due to fiber reinforcing." *Micromechanics of failure of quasi-brittle materials*, S. P. Shah, S. E. Swartz, and M. L. Wang, eds., Elsevier Applied Science, Essex, England, 1–11.
Shah, S. P., Stroeven, P., Dalhuisen, D., and Van Stekelenburg, P. (1979). "Complete stress strain curves for steel fiber reinforced concrete in uniaxial tension and compression." *Proc. RILEM Symp. on Testing and Test Methods of Fiber Cement Composites*, R. M. Swamy, ed., Construction Press Limited, Lancaster, England, 399–408.
Tada, H., Paris, P. C., and Irwin, G. (1973). *The stress analysis of cracks handbook*. Del Research Corp., Hellertown, Pa.
Tandon, G. P., and Weng, G. J. (1986). "Average stress in the matrix and effective moduli of randomly oriented composites." *Compos. Sci. Technol.*, 27, 111–132.
Wakashima, K., and Tsukamoto, H. (1991). "Mean-field micromechanics model and its application to the analysis of thermomechanical behavior of composite materials." *J. Materials science and engineering A.*

Appendix III. Notation

The following symbols are used in this paper:

c = crack radius;
c_{mc} = minimum crack size for which multiple cracking would occur;
c_p = crack radius when maximum bridging stress is reached at crack center;
c_s = crack radius at transition to steady-state crack propagation;
d_f = fiber diameter;

E_c = composite elastic modulus;
E_f = fiber-elastic modulus;
E_m = matrix-elastic modulus;
f = snubbing coefficient;
G_r = energy-absorption rate in fiber-bridging zone behind crack front;
G_{tip} = crack-tip fracture energy-absorption rate;
g = snubbing factor;
K_B = stress-intensity factor due to fiber bridging behind crack tip;
K_L = stress-intensity factor due to applied remote loading;
K_m = matrix-fracture toughness;
K_{tip} = crack-tip–fracture toughness;
L_f = fiber length;
l = fiber-embedment length;
$p(\phi)$ = probability-density function of fiber-orientation angle with respect to loading direction;
$p(z)$ = probability-density function of fiber-centroidal distance from crack-plane critical strain;
δ_m = crack-opening displacement at midpoint of crack;
δ_o = crack opening at which frictional debonding is completed;
δ_p = crack-opening displacement corresponding to maxima of bridging stress;
ε_{ss} = steady-state crack strain;
σ_B = composite bridging stress;
σ_{fc} = first-crack strength;
σ_o = peak bridging stress when $g = 1$;
σ_{ss} = steady-state crack strength; and
τ = interfacial frictional bond strength.